PAPER

A liquid crystalline copper phthalocyanine derivative for high performance organic thin film transistors

Nandu B. Chaure,†*[a] Chandana Pal,[a] Seema Barard,[a] Theo Kreouzis,[a] Asim K. Ray,‡*[a]
Andrew N. Cammidge,*[b] Isabelle Chambrier,[b] Michael J. Cook,*[b] Craig E. Murphy[c] and Markys G. Cain[c]

Bottom-gate, bottom-contact organic thin film transistors (OTFTs) were fabricated using solvent soluble copper 1,4,8,11,15,18,22,25-octakis(hexyl)phthalocyanine as the active semiconductor layer. The compound was deposited as 70 nm thick spin-coated films onto gold source–drain electrodes supported on octadecyltrichlorosilane treated 250 nm thick SiO_2 gate insulators. The performance of the OTFTs was optimised by investigating the effects of vacuum annealing of the films at temperatures between 50 °C and 200 °C, a range that included the thermotropic mesophase of the bulk material. These effects were monitored by ultraviolet-visible absorption spectroscopy, atomic force microscopy and XRD measurements. Device performance was shown to be dependent upon the annealing temperature due to structural changes of the film. Devices heat treated at 100 °C under vacuum ($\geq 10^{-7}$ mbar) were found to exhibit the highest field-effect mobility, 0.7 cm^2 V^{-1} s^{-1}, with an on–off current modulation ratio of ~10^7, a reduced threshold voltage of 2.0 V and a sub-threshold swing of 1.11 V per decade.

1 Introduction

The investigation of small molecule semiconductors is playing a major role in the current rapid development of organic thin film transistors (OTFTs), a technology that ultimately may enable the low cost production of large area light-weight, low-cost printable plastic electronics.[1] Particular issues involve compound design,[2] the development of commercially adaptable solution processing methods for material deposition on flexible substrates,[3] control of molecular alignment within the films for optimisation of the electrical properties,[4] and gaining understanding of the fundamental conduction mechanisms.[5] Semiconductivity exhibited by metallated phthalocyanine macrocycles is well documented[6] and this, coupled with their well-established stability, render them interesting compounds for applications in the area of organic electronics.[7] Early p-type semiconductivity data were largely accrued for unsubstituted derivatives, compounds that have limited solubility in most solvents. These materials are formulated as thin films typically by vapour deposition techniques which are not suitable for large area deposition.

The introduction of substituents onto the phthalocyanine nucleus can confer new and useful properties upon the ring system.[8,9] Thus derivatives bearing eight long alkyl chains at the 1,4,8,11,15,18,22,15-sites (or non-peripheral positions) typically exhibit columnar mesophase behaviour.[9] They are also readily soluble in common organic solvents including tetrahydrofuran, hydrocarbons such as petrol and toluene, and also chlorohydrocarbons such as dichloromethane and chloroform. These materials have proven to be ideal for deposition as well ordered thin films by spin-coating as judged by low angle X-ray reflectivity measurements.[10] Examples have been formulated as spin-coated thin film active layers in two of our laboratories with applications ranging from non-volatile memory devices to biosensors.[11] Elsewhere, a high drift mobility up to 1.4 cm^2 V^{-1} s^{-1} was achieved for holes in the crystal phase of metal-free non-peripherally substituted octahexylphthalocyanine.[12] For all of these reasons, this class of solution processable, low-molecular-weight liquid crystalline phthalocyanine has become a candidate for the semiconducting layer in the design of OTFTs.

We have recently reported the device characteristics of bottom-gate, bottom-contact OTFTs fabricated using spin-coated films of copper 1,4,8,11,15,18,22,25-octahexyl phthalocyanine, **1**, as the active semiconducting layer and the effect of surface passivation of the gate silicon dioxide (SiO_2).[13] When the gate insulator was treated with a self-assembled monolayer of octadecyltrichlorosilane (OTS), an increase in the saturation field effect mobility μ_{sat} by a factor of 20 and simultaneous two orders of magnitude rise in the on–off current ratio were achieved over those obtained without surface passivation. The OTFTs based on **1** showed satisfactory stability to storage in the open laboratory

[a]Centre of Materials Research, Queen Mary, University of London, Mile End Road, London, E1 4NS, UK

[b]School of Chemistry, University of East Anglia, Norwich, NR4 7TJ, UK. E-mail: a.cammidge@uea.ac.uk

[c]National Physical Laboratory, Hampton Road, Teddington, Middlesex, TW11 0LW, UK

† Present address: Department of Physics, University of Pune, Pune 411007, India.

‡ Present address: Wolfson Centre for Materials Processing, Brunel University, Uxbridge, Middlesex UB8 3PH, UK.

This journal is © The Royal Society of Chemistry 2012

J. Mater. Chem., 2012, **22**, 19179–19189 | 19179

environment for 30 days; lack of degradation is an important factor for applications in practical electronics as conventional organic semiconductors such as pentacene and rubrene are known to be prone to instability arising from oxidation.

Compound **1** is known to exhibit thermotropic columnar liquid crystalline behaviour.[14] The purpose of the present work was, therefore, to explore the potential for optimization of the already promising properties of the OTFTs described above *via* the use of thermal annealing. Molecular packing within the films and structural and morphological changes that arise from the annealing process have been examined by ultraviolet-visible absorption spectroscopy, atomic force microscopy (AFM) and X-ray diffraction (XRD). The active layer is expected to be polycrystalline and the electrical performance of OTFT devices is, therefore, expected to be influenced by bulk charge traps, as well as by grain boundary traps of the organic active layer and traps in the interface with the gate insulator.[15] Therefore, the physical interpretation of transistor characteristics has been made in the present investigation by employing a model in which the saturation field effect mobility μ_{sat} is taken to be a charge carrier concentration dependent quantity. The enhanced electrical properties achievable by tuning the active layer structure through annealing the devices under specific conditions are described.

2 Experimental

Copper 1,4,8,11,15,18,22,25-octakis(hexyl)phthalocyanine (**1**) was prepared according to literature methods[16] and its mesophase behaviour as bulk material measured by differential scanning calorimetry (DSC) using a DSC Q20 TA instrument. For spin coating, **1** was dissolved in high purity chloroform and the solution was spin-coated initially at 1000 rpm and finally at 4000 rpm for 20 s and 60 s respectively. Annealing studies of the thin films deposited onto glass were monitored using a Hitachi U-3000 ultraviolet-visible (UV-vis) spectrometer fitted with a Mettler FP80 processor coupled to a Mettler FP82 hot stage.

The drift mobility μ_{dh} was determined from time of flight (TOF) measurement for the hole transport in a 9.1 μm thick film of **1** sandwiched between two transparent indium tin oxide (ITO) coated glass substrates. The cell was formed by slow cooling of the organic layer at a rate of 2 °C min^{-1} to room temperature from the isotropic melt over a film of antiparallel polyimide that was used as the alignment layer. The photocurrents were produced using a 532 nm pulsed output of a frequency-doubled Nd:YAG laser to excite the sample. The bias between the ITO electrodes was provided by a DC power supply while the transient photocurrent was recorded by the voltage drop across the input resistor of a gain 11 amplifier circuit whose output was connected to an Agilent Infinium digitizing oscilloscope. Signal averaging was carried out on all signals in order to improve data quality.[17]

As shown in Fig. 1(b), a bottom gate bottom contact (inverted) OTFT with the ratio of channel width (W) to channel length (L) of 200 was fabricated using a 70 nm thick spin coated film of **1** and 250 nm thick silicon dioxide (SiO$_2$) as the active layer and the gate dielectric layer respectively on a highly doped Si (110) gate electrode. Titanium/gold thin films were made as the source/drain electrodes. The gate SiO$_2$ dielectric was passivated with an OTS self-assembled monolayer. The full protocols of the substrate
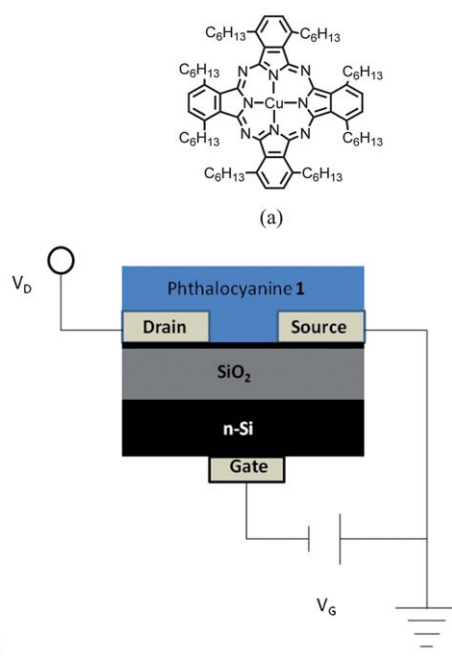
Fig. 1 (a) Chemical structure of **1**. (b) bottom gate bottom contact (inverted) structure.

cleaning, electrode deposition and surface passivation were given in a previous publication.[13]

The OTFT devices were annealed at four different temperatures over the range between 50 °C and 200 °C in a tubular furnace under vacuum of 2×10^{-7} Torr and then gradually cooled down to room temperature at the rate of 1 °C per minute. The surface morphology of the as-prepared and annealed films of **1** was investigated in intermittent contact mode using a Park scanning probe microscope. The atomic force microscopic images (AFM micrographs) of the film surfaces were collected over a scan area of 5 μm × 5 μm for both as-deposited and annealed devices. The effect of high temperature annealing on the crystalline phases of the films of **1** was further examined from XRD patterns acquired at the grazing angle of incidence of 0.3° using a Bruker D8 Advance with Bragg–Brentano geometry scanning in the 2θ range of 5° to 30°, with a step size of 0.02° per second using CuKα radiation of wavelength $\lambda_{CuK\alpha} = 0.15406$ nm. The electrical measurements on these devices were performed at room temperature in air under ambient conditions using a Keithley 4200 semiconductor parameter analyzer.

3 Results and discussion

3.1 Thin film studies

It was established earlier that spin-coated films of zinc metallated 1,4,8,11,15,18,22,25-octakis(alkyl)phthalocyanines undergo molecular reorganizations at temperatures that correspond well to those observed for the crystal to mesophase and mesophase to mesophase transitions that occur in the bulk material.[18] Related macrocycles have been shown to behave similarly.[19] In the present work, we applied comparable experiments to compound **1** to provide insight into the behaviour of films of **1** upon annealing. DSC plots for the first heating, first cooling and second heating components of DSC thermal cycling for compound **1** as the bulk

material are shown in Fig. 2. Transition temperatures are in broad agreement with those in the literature.[20] The first heating cycle reveals some crystal phase–crystal phase transitions at lower temperatures prior to the transition from the crystal (K) to columnar mesophase (C_1) at 180 °C (lit. 184 °C (ref. 20)). The heating component of the second cycle confirms the K–C_1 transition temperature and reveals further mesophase–mesophase transitions at 224.6 °C (C_1–C_2) (not detected previously[20]) and at 233.6 °C (C_2–C_3) (lit. 235.5 °C (ref. 20)) prior to the mesophase to isotropic liquid transition (C_3–I) at 239.9 °C (lit. 242 °C (ref. 20)).

Fig. 3 shows the UV-vis spectrum of a film of **1** supported on a glass slide at room temperature and at 100 °C, 200 °C, 238 °C, and 250 °C. The electronic absorption spectra of phthalocyanines in the solid state are strongly susceptible to exciton coupling effects and these are critically dependent upon molecular packing.[21] The spectrum of the as-deposited spin-coated film of **1** is shown in Fig. 3 as the black line. The visible region absorption, the Q-band envelope, shows two principal absorptions at 710 nm and 641 nm, one to lower energy and one to higher energy relative to the single transition observed at λ_{max} of 706 nm in the solution phase spectrum. Temperature dependent variations in the visible region band envelope of the films, Fig. 3, can be attributed to molecular reorganizations within the film. In a further experiment, variations in absorbance at a selected analytical wavelength, 662 nm, were monitored as the temperature of the film was raised (heating rate 5 °C min^{-1}). This revealed distinct changes in absorbance over small temperature ranges which can be assigned to changes in molecular packing analogous to the mesophase transitions referred to above for the bulk material. Thus transitions detected within the film were observed at 172.5–178.3 °C (corresponding to K–C_1), 225.8–232.5 °C (C_1–C_2 and C_2–C_3) and 235–240 °C (C_3–I).

UV-vis spectroscopy was used further to explore the effect of annealing the 'as-deposited' films for 30 minutes at 50 °C, 100 °C, 150 °C, and 200 °C. In these experiments the films were recorded as-deposited, at the annealing temperature, after 30 min at the annealing temperature, and again after cooling to room temperature. Table 1 reports changes in the λ_{max} of the two main visible region absorptions together with the changes in their absorbance intensities (A) relative to those in the as-deposited film, A_o. The spectra of a film obtained before and after annealing at 50 °C were superimposable. However, those for films annealed at 100 °C and 150 °C show that the annealing process induces minor changes, especially in the relative absorbance intensities of the two bands, $A(1):A(2)$, right hand column in Table 1. Annealing at 200 °C, a temperature within the liquid crystal range of the compound, induces a larger change in the ratio $A(1):A(2)$ as well as a small hysochromic shift of both bands. These results suggest that reorganizations at the molecular level induced by heating the film are relatively small until the films are annealed at 200 °C, i.e. in the mesophase range.

The results of time of flight measurements are shown in Fig. 4(a) in terms of the double logarithmic plots of displacement currents for photogenerated holes. The transit times t_0 of holes traversing the layer of compound **1** were estimated from the inflection points to be 0.95 μs and 0.28 μs for 6 V and 13 V bias, respectively, at room temperature. These yielded values of 0.14 cm^2 V^{-1} s^{-1} and 0.23 cm^2 V^{-1} s^{-1} for mobilities μ_{dh} for 6 V and 13 V, respectively from the relation:[22]

$$\mu_{dh} = \frac{d^2}{V t_0} \tag{1}$$

where d is the cell thickness and V is the applied bias. Further measurements were made for bias voltages between 6 V and 13 V and the results are given in Fig. 4(b) as a Poole–Frenkel plot of μ_{dh} as a function of the square root of the electric field. These values are of the same order of magnitude as those found for metal-free non-peripherally substituted octaoctylphthalocyanine as the bulk material[23] but they are at least two orders of magnitude higher than those measured using the time of flight technique for thermally evaporated copper phthalocyanine.[24] The investigations for larger field strengths were not possible because the inflexion point became engulfed in the initial peak of the photocurrent.

3.2 OTFT characteristics

Fig. 5 shows a set of typical output characteristics for OTFTs with active layers annealed at four different temperatures in terms of drain–source current (I_D) as a function of drain voltage, V_D, for gate voltage, $V_G = -30$ V. For a p-type semiconductor such as compound **1**, an accumulation channel of holes was produced at this gate voltage between the drain and the source in the region near the interface between the dielectric SiO_2 and the active layer. Two similar features of the dependence are observed for all individual devices using differently annealed films of **1** as semiconducting layer. I_D increases linearly within the low V_D regime, implying a uniform charge density in the channel. At higher values of V_D, I_D increased sublinearly with increasing V_D and then saturates at $I_{D(sat)}$. Values of Ohmic conductivity σ_Ω in the inset decrease monotonically with the rise of annealing temperature by a varying degree of magnitude. The values are of the same order of magnitude for temperatures ≤ 100 °C while a four order of magnitude decrease was observed within the temperature regime between 150 °C and 200 °C.

Fig. 6 shows AFM images of the surfaces of the films of **1** within the transistor devices themselves prior to and after annealing. The image in Fig. 6(a) of the as-deposited films shows an apparently void free granular morphology. Annealing at 50 °C caused agglomeration of grains to form small clusters, Fig. 6(b). The cluster size increased on annealing the film at 100 °C producing larger rod-like structures rather than clusters (Fig. 6(c)). The annealing at the higher temperatures of 150 °C and 200 °C gave rise to morphologies containing large plates/slabs as seen in Fig. 6(d) and (e). The films also appeared to contain discontinuities as the cluster sizes became very large. All films were found to have adhered well to the substrate and values of average particle/cluster size along with the root-mean-square roughness data are summarized in Table 2. As given in Table 2, the roughness was found to be as small as 1.6 nm for the rod-like structures in Fig. 6(c) but it increased with the rising annealing temperature of the remaining films. The average cluster size was found to increase monotonically from 0.2 μm for an as-deposited film to ∼2.0 μm for the film annealed at 200 °C. XRD patterns (Fig. 7) obtained for similarly annealed active layers exhibit multiple diffraction peaks, indicating the polycrystalline structure of the films. As the annealing temperature was increased from 50 °C to 150 °C, the peaks became sharper with decreased
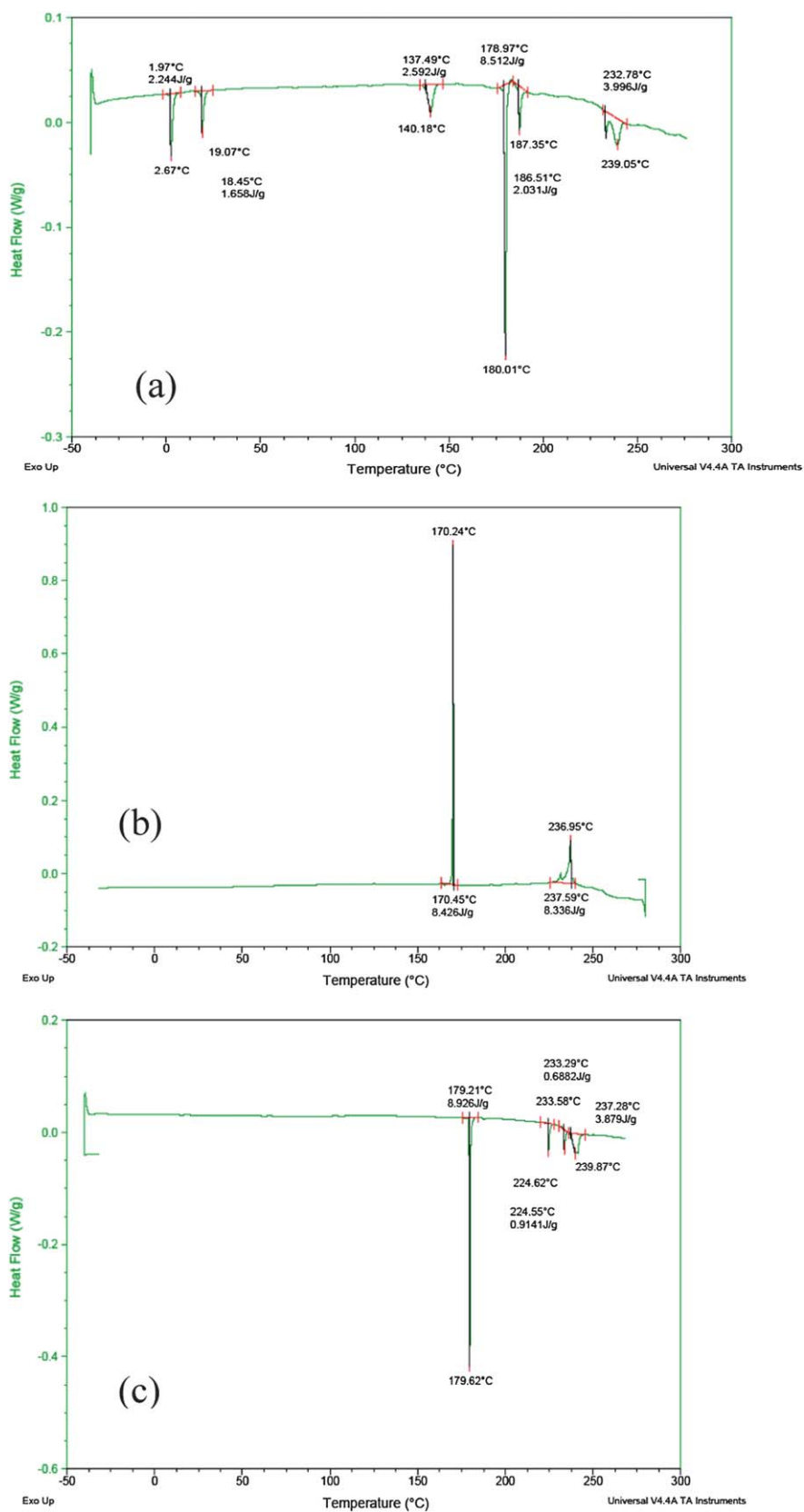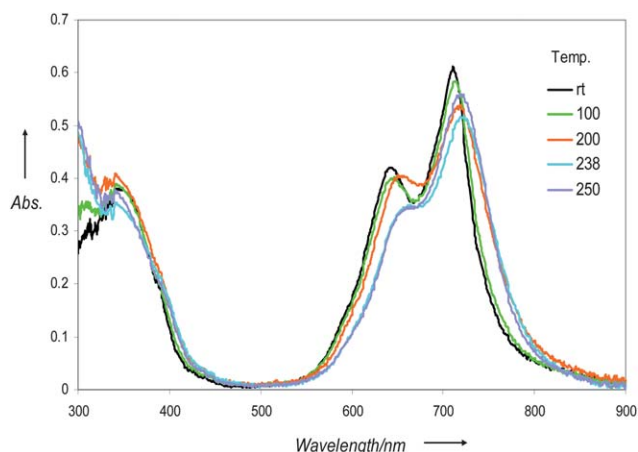
Fig. 2 (a) DSC curve of **1** on the heating component of first cycle. (b) DSC curve on subsequent cooling. (c) DSC curve for the second heating step.

This journal is © The Royal Society of Chemistry 2012

Fig. 3 UV-visible spectra of a spin-coated film of **1** measured at room temperature, 100 °C, 200 °C, 238 °C and 250 °C.

full width at half maxima (FWHM). The films annealed at 100 °C gave peaks at $2\theta = 7.90°$ and $2\theta = 11.93°$ corresponding to the d-spacing of 1.12 nm and 0.74 nm, respectively, and are similar to those obtained for tetraoctyl-substituted vanadyl phthalocyanine thin films annealed at 120 °C indicating the edge-on alignment of the molecules.[25] The plot of $\beta \cos\theta$ against $\sin\theta$ in the inset is found to be linear, indicating the validity of the Williamson–Hall equation in the form:[26]

$$\beta \cos \theta = 4\eta \sin \theta + \frac{K\lambda_{\text{Cuk}\alpha}}{D} \qquad (2)$$

where β is FWHM at the Bragg angle θ and K is constant with a value of 0.94. Values of the strain η and the mean grain size D were estimated from the slope and intercept, respectively, for all five devices. The dislocation density (δ) which is defined as the length of dislocation lines per unit value of crystal can be estimated as $\delta = D^{-2}$. The results are summarised in Table 2. The decrease of FWHM with annealing temperature (seen in Fig. 7) may be attributed to the reduction in the concentration of lattice
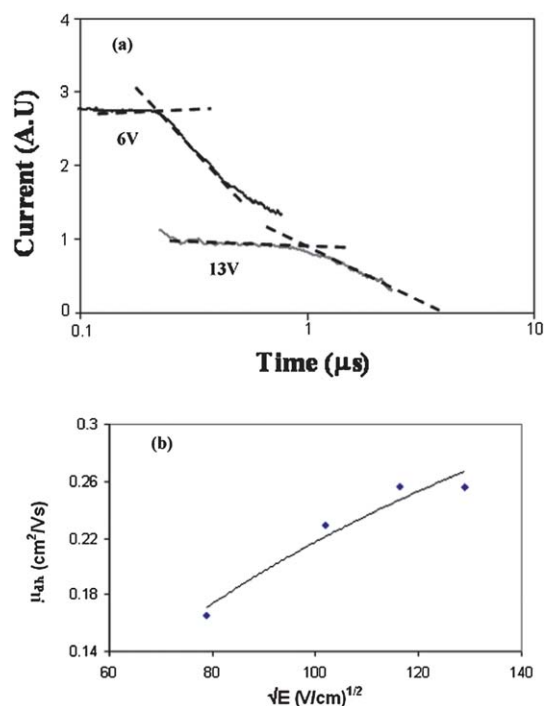
Fig. 4 (a) Hole photocurrent transients in a 9.1 μm thick cell of **1** at the applied bias of 6 V and 13 V scaling correctly with field and (b) hole mobilities in **1** parametric in electric field.

imperfections, due to the increase in the mean grain size. Similarly, the strain η decreases with larger grain size and this compressive stress is due to the grain boundary effect, which is predominant in polycrystalline films.

The AFM and XRD studies therefore imply that the difference in the annealing temperature dependent OTFT characteristics may be attributed to the sizes, boundaries and orientations of the clusters in the active layer. The quantitative examination of the dependence of the OTFT characteristics on the grain boundaries of the active layer of **1** was made from the Levinson plots in

Table 1 Variations in the absorption maxima (nm) and relative absorbances (A:A) of the two main visible region bands during the annealing cycles of the film of **1**

Annealing temperature and cycle		(1) $\lambda_{\max}$/nm	$A(1):A_o{}^a$	(2) $\lambda_{\max}$/nm	$A(2):A_o{}^a$	$A(1):A(2)$
50 °C	Room temperature	710	1	641	1	1.443
	50 °C	711	0.97	642	0.97	1.438
	50 °C (after 30 min)	711	0.98	642	0.98	1.440
	Back to room temperature	710	1	641	1	1.443
100 °C	Room temperature	711	1	641	1	1.387
	100 °C	713	0.94	643	0.94	1.386
	100 °C (after 30 min)	713	0.93	643	0.94	1.371
	Back to room temperature	710	1	640	1	1.369
150 °C	Room temperature	710	1	640	1	1.426
	150 °C	714	0.86	645	0.88	1.392
	150 °C (after 30 min)	714	0.84	645	0.87	1.365
	Back to room temperature	710	0.88	640	0.94	1.339
200 °C	Room temperature	710	1	641	1	1.430
	200 °C	716	0.8	653	0.9	1.265
	200 °C (after 30 min)	716	0.78	652	0.88	1.269
	Back to room temperature	708	0.87	638	0.98	1.273

[a] A_o refers to the absorbance of the band in the as-deposited, *i.e.* non annealed, film.
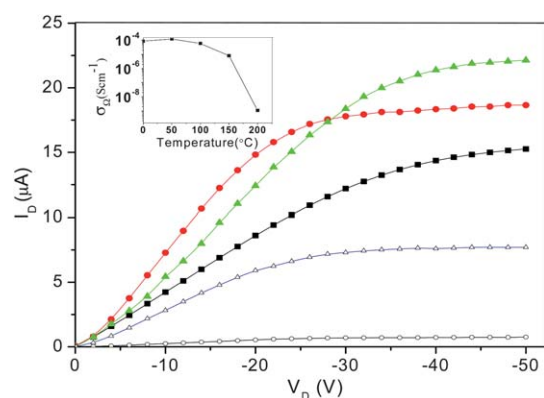
Fig. 5 Dependence of output characteristics for the source-to-gate voltage ($V_{GS} = -30$ V) on the annealing temperature of the film of **1**: as-deposited (solid rectangle), 50 °C (solid circle), 100 °C (solid triangle), 150 °C (open triangle) and 200 °C (open circle).

Fig. 8 of $\ln(I_D/V_G)$ *vs.* $1/V_G$ for $V_D = -5$ V. The linear graphs show the dependence of I_D on the density N_g of traps at the grain boundaries of the phthalocyanine layer in the form:[27]

$$I_D = \mu_{GB0} V_D \frac{W}{L} C_i V_G \exp\left(- \frac{q^3 N_g^2 t}{8\varepsilon_0 \varepsilon_{pc} kT C_i V_G} \right) \qquad (3)$$

where the trap-free mobility in the grain boundary μ_{GB0} usually depends on the grain size and the carrier concentration, but only slightly on measurement temperature. Values of N_g and μ_{GB0} were determined from the slope and the extrapolation for $1/V_G \rightarrow 0$; the results are summarized in Table 3. Free space permittivity $\varepsilon_0 = 8.85 \times 10^{-12}$ F m^{-1}, electronic charge $q = 1.6 \times 10^{-19}$ C, Boltzmann constant $k = 8.62 \times 10^{-5}$ eV K^{-1}, temperature $T = 300$ K and dielectric constant $\varepsilon_{pc} = 3$ of **1** were used for the calculations of N_g from eqn (3). The value of C_i for the OTS treated SiO$_2$ gate insulator was taken to be 1×10^{-4} F m^{-2}.[13] As expected, values of μ_{GB0} remain virtually the same for the films which were annealed at a temperature ≤ 100 °C. However, an order of magnitude decrease was observed for μ_{GB0} as a result of
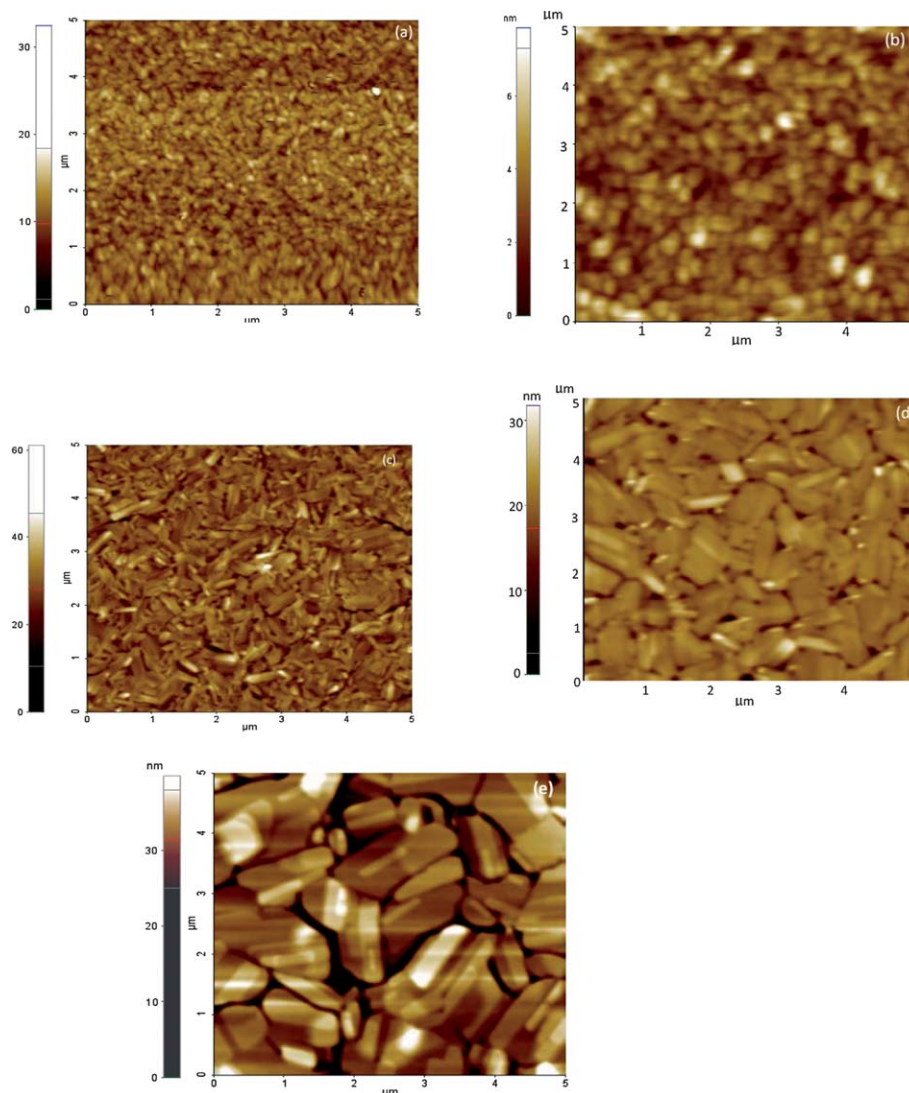
Fig. 6 AFM images of **1** films. (a) as-deposited and annealed for 30 minutes at (b) 50 °C (c) 100 °C, (d) 150 °C, (e) 200 °C.

Table 2 Results from AFM and XRD studies

| Annealing temperature (°C)	AFM		XRD		
	Average particle/cluster size (μm)	Roughness (nm)	Average grain size (D) (nm)	Dislocation density (δ) ($\times 10^{14}$ m^{-2})	Strain (η) ($\times 10^{-3}$)
As-prepared	0.2	2.5	17	34.6	36.0
50	0.5	3.3	24	17.4	4.7
100	0.8	1.6	62	2.60	6.4
150	1.0	4.5	52	3.70	7.1
200	2.0	7.9	Amorphous		

higher annealing temperatures. The values of N_g are of the same order of magnitude for all annealing temperatures.

The transfer characteristic in Fig. 9 of drain–source current $I_{D(sat)}$ *versus* gate voltage V_G for drain–source voltage $V_D = -40$ V exhibits high on–off current ratios varying from 10^5 for an OTFT annealed at 200 °C to 10^7 for annealing at 100 °C (shown in Table 3). The density N_{SS} of traps at the interface between the organic layer and the gate SiO$_2$ dielectrics is related to the sub-threshold voltage swing S in the form:[28]
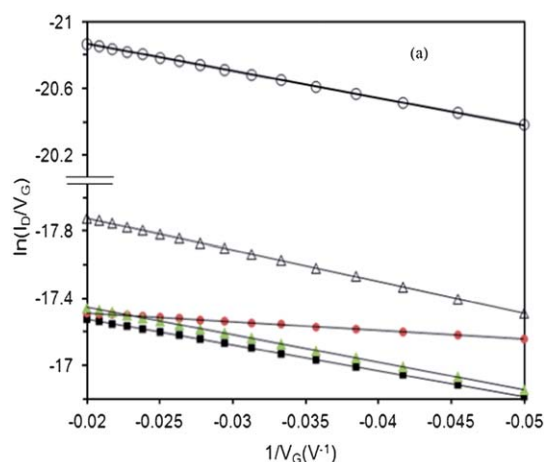
$$N_{ss} = \left[\frac{S \log(e)}{kT} - 1\right] \frac{C_i}{q} \tag{4}$$

The sub-threshold voltage swing S, defined as the voltage V_G required to increase I_D by a factor of 10, was estimated using the formula in the form:

$$S = \frac{dV_G}{d(\log I_D)} \tag{5}$$
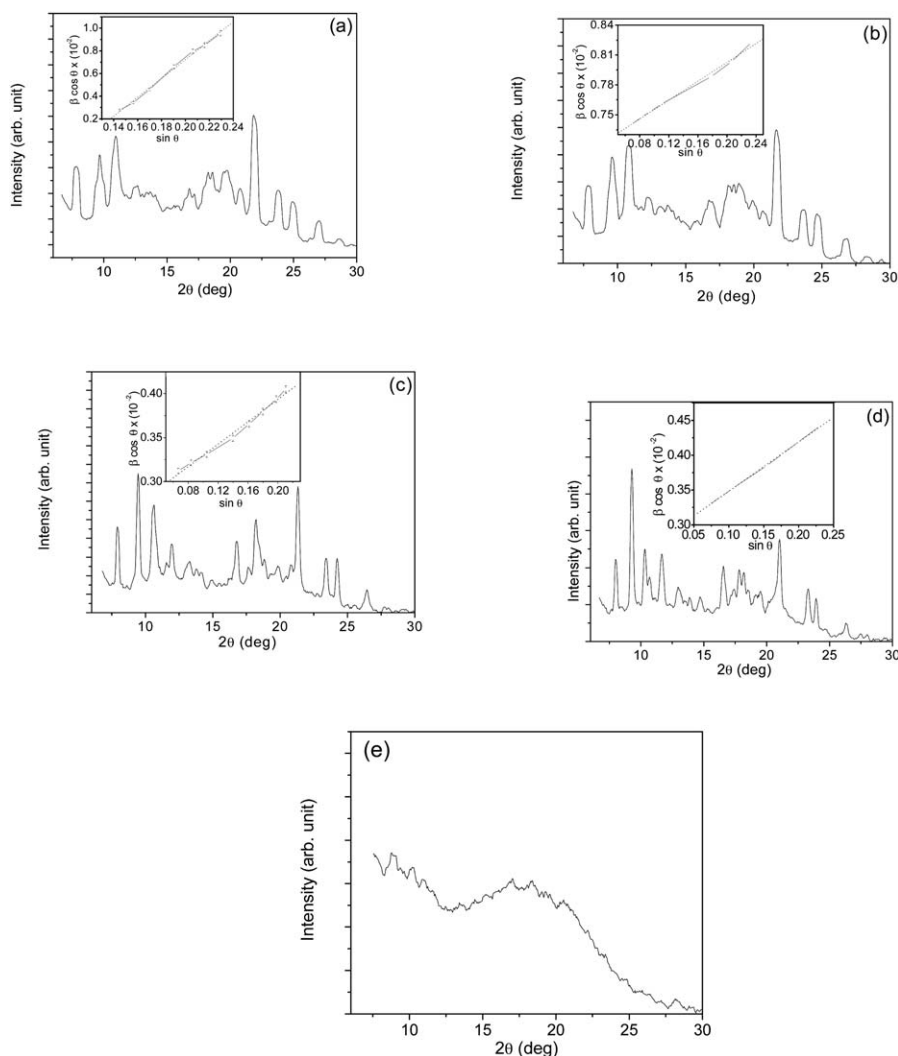
Fig. 7 XRD patterns of **1** films (a) as-deposited and annealed for 30 minutes at (b) 50 °C (c) 100 °C, (d) 150 °C, (e) 200 °C. Inset shows the plots of Williams–Hall equations.
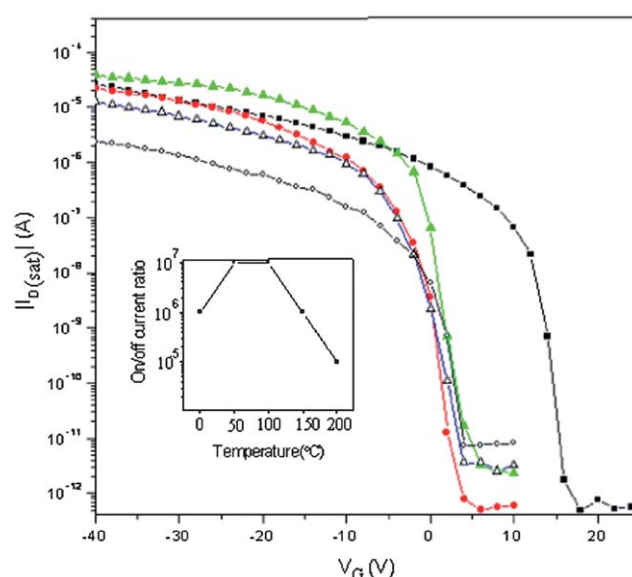
Fig. 8 Levinson plot of $\ln(I_D/V_G)$ as function n of $1/V_G$ for $V_D = -5$ V, for transistors with **1** as active layer annealed at different temperatures: as deposited (solid rectangle), 50 °C (solid circle), 100 °C (solid triangle), 150 °C (open triangle) and 200 °C (open circle).

As shown in Table 3, values of S and N_{SS} estimated for OTFTs using the copper phthalocyanine derivative **1** as the active layer are found to remain within the same order of magnitude. Therefore, it can be assumed that the interfacial characteristics between the amphiphilic OTS molecules and both phthalocyanine films and hydrophilic SiO$_2$ remained unaffected by post thermal treatment of the films of **1**. The OTFT annealed at 100 °C showed the smallest trap density of 9.8×10^{15} eV^{-1} m^{-2} corresponding to a value of $S = 1.11$ V per decade.

The dependence of the saturation current $I_{D(sat)}$ on V_G for disordered OTFTs is described by the relationship:

$$I_D = \beta_{TFT}(V_G - V_T)^{2T_c/T} \tag{6}$$

where V_T is the threshold voltage. β_{TFT} is a constant depending upon the aspect ratio, gate capacitance C_i, saturation field effect mobility μ_{sat} and carrier density ρ. T_C is the characteristic temperature associated with the width of the Gaussian or slope of the exponential distribution of traps.[29] Values of T_C and V_T were determined from the slope and the intercept of the linear fit in Fig. 10 to the relation in the form:

Fig. 9 Transfer characteristics I_D as a function of V_G for $V_D = -40$ V for transistors with **1** as active layer annealed at different temperatures: as-deposited (solid rectangle), 50 °C (solid circle), 100 °C (solid triangle), 150 °C (open triangle) and 200 °C (open circle). Inset shows dependence of on–off current ratio on annealing temperature.

$$\frac{I_{D(sat)}}{(\partial I_{D(sat)}/\partial V_G)} = \frac{T}{2T_c}(V_G - V_T) \tag{7}$$

It is found from Table 3 that the annealed OTFTs switched on at relatively low threshold voltages compared to the devices using as-prepared semiconductor films. The shift in V_T is believed to be due to the bulk trap limited charge transport in the organic layer and its value is related to the square root of the density N_B of these traps in the form:[30]

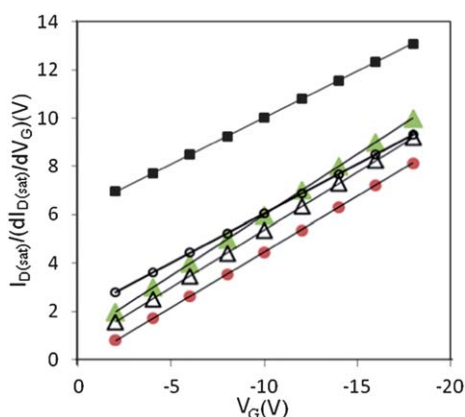$$N_B = \frac{V_T^2 C_i^2}{2\varepsilon_{pc}\varepsilon_0 kT} \tag{8}$$

Values of N_B given in Table 3 are believed to be dependent upon the combined effect of the grain size and roughness of the films. The film annealed at 100 °C is estimated to have the smallest density of the bulk trap with the lowest roughness.

Values of β_{TFT} were obtained from the slope of linear extrapolation of the plots of $(I_{D(sat)})^{(1/2m+2)}$ as V_G in Fig. 11 according to the relation:[31]

Table 3 Organic thin film transistor device characteristics constructed using compound **1**

Annealing temperature (°C)	Mobility (cm^2 V^{-1} s^{-1})		On–off current ratio	V_T (V)	S (V per decade)	Trap parameters				
	$\mu_{GBO} \times 10^{-2}$	μ_{sat}				Distribution characteristics		Density		
						T_c (K)	E_{MN} (meV)	N_{ss} (eV^{-1} cm^{-2}) $\times 10^{12}$	N_g (cm^{-2}) $\times 10^{11}$	N_B (cm^{-3}) $\times 10^{17}$
As-prepared	0.29	0.08	1.2×10^6	−16	1.45	392	33.78	1.30	2.13	7.35
50	0.31	0.12	7.6×10^7	−2	1.22	327	28.18	1.10	1.23	0.92
100	0.28	0.70	8.4×10^7	−1	1.11	300	25.86	0.98	2.19	0.46
150	0.05	0.03	6.8×10^6	−1.3	1.59	315	27.14	1.44	2.36	0.59
200	0.01	0.01	1.3×10^5	−5	1.74	369	31.79	1.64	2.18	2.29

Fig. 10 Plots of $\dfrac{I_{D(sat)}}{(\partial I_{D(sat)}/\partial V_G)}$ against V_G for $V_D = -40$ V: as deposited (solid rectangle), 50 °C (solid circle), 100 °C (solid triangle), 150 °C (open triangle) and 200 °C (open circle).

$$\beta = \frac{W}{L}\frac{\mu_{sat}^{1-m}C_i^{2m+1}}{(2m+1)(2m+2)(2\varepsilon_0\varepsilon_{pc}qkT)^m}\left(\frac{I_{DS(sat)}}{V_{DS}}\frac{L}{Wt}\right)^m \quad (9)$$

The power exponent m which determines the degree of disorder of the structure of the active film of **1** is related to the temperature T_C through the relation:

$$m = \frac{T_C}{T} - 1 \quad (10)$$

When $T_C = T$, $m = 0$ and under these circumstances, eqn (6) indicates the square law dependence of $I_{D(sat)}$ on V_G, similar to one used for the transistors with a single crystal material as an active layer.

Using eqn (9) and (10), values of μ_{sat} were estimated as a function of annealing temperature. As shown in the inset of Fig. 11, there is a good correlation between T_C and μ_{sat} indicating the presence of Meyer–Neldel behaviour.[32] Earlier transmission electron microscopy (TEM) studies on spin coated films of a number of phthalocyanine analogues of **1** indicate that during the evaporation process the molecules assemble to form columnar structures.[33] This process presumably also arises
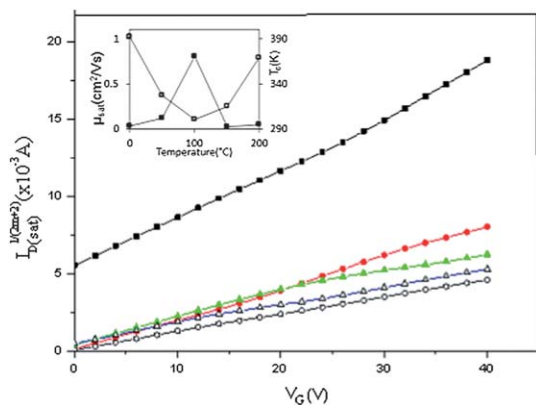
Fig. 11 Plots of $I_{D(sat)}^{1/(2m+2)}$ against V_G for $V_D = -40$ V: as deposited (solid rectangle), 50 °C (solid circle), 100 °C (solid triangle), 150 °C (open triangle) and 200 °C (open circle). Dependence of μ_{sat} (solid square) and T_c (open square) on annealing temperature are shown in inset.
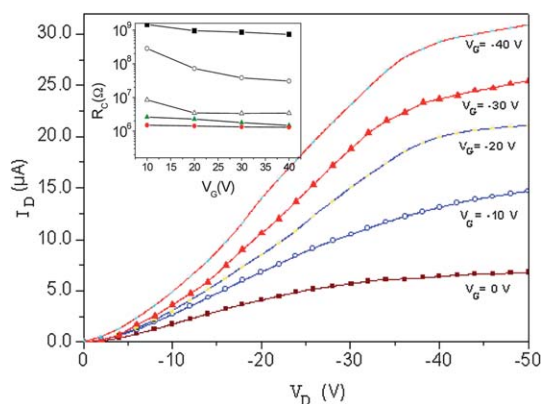
during the fabrication of spin coated films of **1**. X-ray diffraction measurements indicated that they were comprised of layers of columns whose axes are parallel to the surface of the substrate, *i.e.* with the molecules arranged 'edge-on' to the surface. Such an arrangement is expected to be conducive to one dimensional flow of current I_D between the drain and the source near the interface with the gate insulator through overlap of π–π molecular orbitals within the columnar stacks. However, it is evident from the AFM images and XRD patterns described earlier that the channel is not a single crystalline structure. The films annealed at different temperatures are expected to contain high density of traps with characteristic Meyer–Neldel energies E_{MN} ($= kT_C$) of the exponential tail states distributed between 33.8 meV and 25.9 meV (Table 3). For the ratio of $\dfrac{E_{MN}}{kT} \neq 1$, eqn (10) suggests that trapped charges do not contribute to the drain to source current and therefore the mobility μ_{sat} becomes dependent upon the ratio of trapped-to-free carriers controlled by the gate bias. For the film annealed at 100 °C, $E_{MN} \approx kT$ and the ratio of trapped-to-free carriers is small as for a nearly perfect crystalline film, giving the highest value of μ_{sat}. The Meyer–Neldel behaviour has been observed in space charge limited conduction through thermal evaporated fluorinated copper phthalocyanine films and the trap characteristics are believed to be associated with the structure disorder inherent with the vacuum preparation.[34] Similarly, the disorder features in the active layer of **1** may be attributed to the thermal annealing process in the present investigation. It has also been reported that the improved control of the organic film morphology can be achieved by laser annealing at low temperature.[35] Compound **1** also exhibits strong anisotropic charge transport in the direction of the discotic stacking direction because the values of the mobility obtained in the present work from the time of flight and field effect measurements are different. Similar anisotropic conduction behaviour has been observed for 2(3),9(10),16(17),23(24)-tetra(2-decyltetradecyloxy) metal-free phthalocyanine. However, the mobility obtained from time of flight and field effect experiments was very low, in the range between 10^{-3} cm² V⁻¹ s⁻¹ and 10^{-7} cm² V⁻¹ s⁻¹.[36]

The Fermi level of gold is typically about 0.7 eV above the highest occupied molecular orbital level (HOMO) of a copper phthalocyanine derivative.[37] The active phthalocyanine layer formed Schottky type contacts with both source and drain electrodes. It can be seen from the output characteristics in Fig. 12, of the OTFT annealed at 100 °C, that the rise of I_D with increasing V_D at low bias is small due to significant reduction in injection of carriers through the wide barrier at the source electrode. The effective contact resistance R_C is written in the form:[38]

$$R_c = \frac{V_D}{I_D} - \frac{L}{\mu_{eff}WC_i}\frac{1}{(V_G - V_T)^{\left(\frac{2T_C}{T} = 1\right)}} \quad (11)$$

where the effective mobility μ_{eff} is estimated from Fig. 8.

As shown in the inset of Fig. 12, values of R_C for OTFTs were found to decrease with increasing the gate voltage V_G indicating that the potential barrier at the forward-biased source electrode became sufficiently narrow resulting in increased tunneling current. Since the gold electrodes were covered by the film of **1** in a bottom-gate configuration, the decrease in R_C on annealing of

This journal is © The Royal Society of Chemistry 2012

J. Mater. Chem., 2012, **22**, 19179–19189 | 19187

Fig. 12 Output characteristics for gate voltage V_G ($-40V \leq V_G \leq 0$ V). for the transistor with **1** as active layer annealed at 100 °C. Inset shows the dependence of the contact resistance R_C on V_G for active layer annealed at different temperatures: as-deposited (solid rectangle), 50 °C (solid circle), 100 °C (solid triangle), 150 °C (open triangle) and 200 °C (open circle).

the active layers is believed to be primarily related to the degree of the film crystallinity as seen previously in the XRD patterns in Fig. 7. Values of R_C for OTFT annealed at 100 °C are smaller than that of the as-deposited transistor by approximately three orders of magnitude.

4. Conclusion

The annealing temperature of the active layer of copper phthalocyanine **1** is found to have produced a significant effect upon the transistor performance of the OTFT. Molecules are well aligned in the spin-coated film with their columnar axis parallel to the substrate. The drain–source current is believed to be one dimensional hole transport *via* the overlap of π–π molecular orbitals through the accumulation layer. Although no noticeable changes in the molecular packing due to thermal annealing have been observed by optical absorption spectroscopy unless the temperature was raised to 200 °C, a disordered film structure is evident from AFM images which reveal an annealing temperature dependent growth of crystallites in different shapes, sizes and orientations. This gives rise to the variation in the characteristic Meyer–Neldel energy for the width of the tails of exponentially distributed traps. For the film annealed at 100 °C the Meyer–Neldel energy is close to the thermal energy at room temperature implying that the morphology of highly packed rod-like crystallite structure with good grain interconnectivity produces a nearly single crystalline field effect behaviour. Therefore, the OTFTs using the annealed layer at this temperature produce the transistor parameters in terms of on–off ratio, and field-effect mobility comparable to those reported for small molecule transistors.

References

1 (*a*) D. Tobjork and R. Osterbacka, *Adv. Mater.*, 2011, **23**, 1935–1961; (*b*) D. S. Weiss and M. Abkowitz, *Chem. Rev.*, 2010, **110**, 479–526; (*c*) T. Mori, *J. Phys.: Condens. Matter*, 2008, **20**, 184010; (*d*) C. A. Di, G. Yu, Y. Liu and D. Zhu, *J. Phys. Chem. B*, 2007, **111**, 14083–14096; (*e*) A. Dodabalapur, *Mater. Today*, 2006, **9**, 24–30; (*f*) T. B. Singh and N. S. Sariciftci, *Annu. Rev. Mater. Res.*, 2006, **36**, 199–230.

2 (*a*) B. Lucas, T. Trigaud and C. Videlot-Ackermann, *Polym. Int.*, 2012, **61**, 374–389; (*b*) F. S. Kim, G. Q. Ren and S. A. Jenekhe, *Chem. Mater.*, 2011, **23**, 682–732; (*c*) X. W. Zhan, A. Facchetti, S. Barlow, T. J. Marks, M. A. Ratner, M. R. Wasielewski and S. R. Marder, *Adv. Mater.*, 2011, **23**, 268–284; (*d*) B. R. Kaafarani, *Chem. Mater.*, 2011, **23**, 378–396.

3 (*a*) Y. Li, C. Liu, Y. Xu, T. Minari, P. Darmawan and K. Tsukagoshi, *Org. Electron.*, 2012, **13**, 815–819; (*b*) K. H. Shin, J. Cho, J. Jang, H. S. Jang, E. S. Park, K. Song and S. H. Kim, *Org. Electron.*, 2012, **13**, 715–720; (*c*) M. C. Rosamond, A. J. Gallant, M. C. Petty, O. Kolosov and D. A. Zeze, *Adv. Mater.*, 2011, **23**, 5039–5044; (*d*) J. L. Yang and D. H. Yan, *Chem. Soc. Rev.*, 2009, **38**, 2634–2645; (*e*) T. Kawase, S. Moriya, C. J. Newsome and T. Shimoda, *Jpn. J. Appl. Phys., Part 1*, 2005, **44**, 3649–3658.

4 (*a*) S. H. Liu, W. C. M. Wang, A. L. Briseno, S. C. E. Mannsfeld and Z. N. Bao, *Adv. Mater.*, 2009, **21**, 1217–1232; (*b*) T. Wang, L. Z. Huang, J. L. Yang, H. K. Tian, Y. H. Geng and D. H. Yan, *J. Phys. Chem. B*, 2010, **114**, 16408–16413; (*c*) S. Chakrabarti, S. Dey and A. J. Pal, *Appl. Phys. Lett.*, 2011, **99**, 053308; (*d*) Y. J. Yun, C. Pearson and M. C. Petty, *J. Appl. Phys.*, 2009, **105**, 034508.

5 (*a*) H. Sirringhaus, M. Bird, T. Richards and N. Zhao, *Adv. Mater.*, 2010, **22**, 3893–3898; (*b*) I. I. Fishchuk, A. K. Kadashchuk, J. Genoe, M. Ullah, H. Sitter, T. B. Singh, N. S. Sariciftci and H. Baessler, *Phys. Rev. B: Condens. Matter Mater. Phys.*, 2010, **81**, 045202; (*c*) N. Tessler, Y. Preezant, N. Rappaport and Y. Roichman, *Adv. Mater.*, 2009, **21**, 2741–2761; (*d*) S. Kera, H. Yamane and N. Ueno, *Prog. Surf. Sci.*, 2009, **84**, 135–154; (*e*) M. E. Gershenson, V. Podzorov and A. F. Morpurgo, *Rev. Mod. Phys.*, 2006, **78**, 973–989.

6 (*a*) R. Hayakawa, N. Hiroshiba, T. Chikyow and Y. Wakayama, *Adv. Funct. Mater.*, 2011, **21**, 2933–2937; (*b*) D. Schlettwein, N. I. Jaeger and T. Oekermann, in *The Porphyrin Handbook*, ed. K. M. Kadish, K. M. Smith and R. Guillard, Academic Press, San Diego, 2003, vol. 16, pp. 247–283; (*c*) M. Hanack and D. Dini, in *The Porphyrin Handbook*, ed. K. M. Kadish, K. M. Smith and R. Guilard, Academic Press, San Diego, 2003, vol. 18, pp. 251–280.

7 (*a*) L. Jiang, H. L. Dong and W. P. Hu, *J. Mater. Chem.*, 2010, **20**, 4994–5007; (*b*) S. P. Singh, A. Sellinger and A. Dodabalapur, *J. Appl. Phys.*, 2010, **107**, 044509; (*c*) G. Witte and C. Woll, *J. Mater. Res.*, 2004, **19**, 1889–1916; (*d*) C. D. Dimitrakopoulos and P. R. L. Malenfant, *Adv. Mater.*, 2002, **14**, 99–117.

8 (*a*) Y. Shimizu, Y. Matsuda, F. Nekelson, H. Miyake, H. Yoshida, A. Fujii and M. Ozaki, *Proc. SPIE*, 2012, **8279**, 82790G; (*b*) D. J. Tate, R. Anemian, R. J. Bushby, S. Nanan, S. L. Warriner and B. J. Whitaker, *Beilstein J. Org. Chem.*, 2012, **8**, 120–128; (*c*) E. A. Lukyanets and V. N. Nemykin, *J. Porphyrins Phthalocyanines*, 2010, **14**, 1–40; (*d*) J. Z. Jiang, L. Bao, L. Rintoul and D. P. Arnold, *Coord. Chem. Rev.*, 2006, **250**, 424–448.

9 M. J. Cook and I. Chambrier, *J. Porphyrins Phthalocyanines*, 2011, **15**, 149–173.

10 S. M. Critchley, M. R. Willis, M. J. Cook, J. McMurdo and Y. Maruyama, *J. Mater. Chem.*, 1992, **2**, 157–159.

11 (*a*) B. Mukherjee, A. K. Ray, A. K. Sharma, M. J. Cook and I. Chambrier, *J. Appl. Phys.*, 2008, **103**, 074507; (*b*) S. Sahu, A. K. Sharma, M. J. Cook and A. K. Ray, *J. Mater. Sci.: Mater. Electron.*, 2010, **21**, 567–570; (*c*) N. B. Chaure, J. L. Sosa-Sanchez, A. N. Cammidge, M. J. Cook and A. K. Ray, *Org. Electron.*, 2010, **11**, 434–438; (*d*) C. Pal, A. N. Cammidge, M. J. Cook, J. L. Sosa-Sanchez, A. K. Sharma and A. K. Ray, *J. R. Soc. Interface*, 2012, **9**, 183–189.

19188 | *J. Mater. Chem.*, 2012, **22**, 19179–19189

This journal is © The Royal Society of Chemistry 2012

12 Y. Miyake, Y. Shiraiwa, K. Okada, H. Monobe, T. Hori, N. Yamasaki, H. Yoshida, M. J. Cook, A. Fujii, M. Ozaki and Y. Shimizu, *Appl. Phys. Express*, 2011, **4**, 021604.

13 N. B. Chaure, A. N. Cammidge, I. Chambrier, M. J. Cook, M. G. Cain, C. E. Murphy, C. Pal and A. K. Ray, *Sci. Technol. Adv. Mater.*, 2011, **12**, 025001.

14 M. J. Cook, S. J. Cracknell and K. J. Harrison, *J. Mater. Chem.*, 1991, **1**, 703–704.

15 J. Rivnay, L. H. Jimison, J. E. Northrup, M. F. Toney, R. Noriega, S. F. Lu, T. J. Marks, A. Facchetti and A. Salleo, *Nat. Mater.*, 2009, **8**, 952–958.

16 N. B. McKeown, I. Chambrier and M. J. Cook, *J. Chem. Soc., Perkin Trans. 1*, 1990, 1169–1177.

17 S. Barard, M. Heeney, L. Chen, M. Colle, M. Shkunov, I. McCulloch, N. Stingelin, M. Philips and T. Kreouzis, *J. Appl. Phys.*, 2009, **105**, 013701.

18 M. J. Cook, D. A. Mayes and R. H. Poynter, *J. Mater. Chem.*, 1995, **5**, 2233–2238.

19 A. N. Cammidge, I. Chambrier, M. J. Cook, E. H. G. Langner, M. Rahman and J. C. Swarts, *J. Porphyrins Phthalocyanines*, 2011, **15**, 890–897.

20 A. S. Cherodian, A. N. Davies, R. M. Richardson, M. J. Cook, N. B. McKeown, A. J. Thomson, J. Feijoo, G. Ungar and K. J. Harrison, *Mol. Cryst. Liq. Cryst.*, 1991, **196**, 103–114.

21 (a) M. J. Cook, in *Spectroscopy of New Materials: Advances in Spectroscopy*, ed. R. J. H. Clark and R. E. Hester, Wiley, Chichester, 1993, vol. 22, pp. 87–150; (b) A. K. Ray, A. V. Nabok, A. K. Hassan, O. Omar, R. Taylor and M. J. Cook, *Philos. Mag. B*, 1998, **78**, 53–64.

22 J. Wu, T. Usui and J. Hanna, *J. Mater. Chem.*, 2011, **21**, 8045–8051.

23 H. Iino, J. Hanna, R. J. Bushby, B. Movaghar, B. J. Whitaker and M. J. Cook, *J. Appl. Phys.*, 2005, **87**, 132102.

24 (a) H. Fujikake, T. Murashige, M. Sugibayashi and K. Ohta, *Appl. Phys. Lett.*, 2004, **85**, 3474–3476; (b) M. Kitamura, T. Imada, S. Kako and A. Arakawa, *Jpn. J. Appl. Phys.*, 2004, **43**, 2326–2329.

25 S. Q. Dong, H. K. Tian, D. Song, Z. H. Yang, D. H. Yan, Y. H. Geng and F. S. Wang, *Chem. Commun.*, 2009, 3086–3088.

26 G. K. Williamson and W. H. Hall, *Acta Metall.*, 1953, **1**, 22–31.

27 J. Levinson, F. R. Shepherd, P. R. Scanlon, W. D. Westwood, G. Este and M. Rider, *J. Appl. Phys.*, 1982, **53**, 1193–1202.

28 A. R. Brown, C. P. Jarrett, D. M. deLeeuw and M. Matters, *Synth. Met.*, 1997, **88**, 37–55.

29 M. K. Rabinal and K. L. Narasimhan, *Philos. Mag. B*, 2000, **80**, 113–123.

30 J. H. Schon and B. Batlogg, *J. Appl. Phys.*, 2001, **89**, 336–342.

31 M. Raja and W. Eccleston, *IET Circuits, Devices and Systems*, 2012, **6**, 122–129.

32 W. Meyer and H. Neldel, *Z. Tech. Phys.*, 1937, **12**, 588.

33 M. J. Cook, *Chem. Rec.*, 2002, **2**, 225–236.

34 J. H. Schon and Z. A. Bao, *J. Appl. Phys.*, 2001, **89**, 3526–3528.

35 K. Kubota, T. Kato and C. Adachi, *Appl. Phys. Lett.*, 2009, **95**, 073303.

36 C. Deibel, D. Janssen, P. Heremans, V. De Cupere, Y. Geerts, M. L. Benkhedir and G. J. Adriaenssens, *Org. Electron.*, 2006, **7**, 495–499.

37 M. Kraus, S. Richler, A. Opitz, W. Bruetting, S. Haas, T. Hasegawa, A. Hinderhofer and F. Schreiber, *J. Appl. Phys.*, 2010, **107**, 094503.

38 D. Natali, L. Fumagalli and M. Sampietro, *J. Appl. Phys.*, 2007, **101**, 014501.

This journal is © The Royal Society of Chemistry 2012

J. Mater. Chem., 2012, **22**, 19179–19189 | 19189